Applied Surface Science 638 (2023) 158076

Contents lists available at ScienceDirect

Applied Surface Science

journal homepage: www.elsevier.com/locate/apsusc

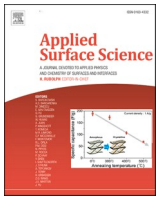

Full Length Article

An *in situ* ToF-LEIS characterization of the surface of Ti-based thin films under oxygen exposure and at elevated temperatures

Philipp M. Wolf [a,*], Deborah Neuß [b], Tuan T. Tran [a], Eduardo Pitthan [a], Marcus Hans [b], Jochen M. Schneider [b], Daniel Primetzhofer [a,c]

[a] Department of Physics and Astronomy, Ångström Laboratory, Uppsala University, Box 516, SE-751 20 Uppsala, Sweden
[b] Materials Chemistry, RWTH Aachen University, Kopernikusstr. 10, D-52074 Aachen, Germany
[c] Tandem Laboratory, Uppsala University, Uppsala, Sweden

ARTICLE INFO

Keywords:
Time-of-flight low-energy ion scattering
Surface analysis
High-resolution depth profiling
Titanium
Transition metal nitride
In situ

ABSTRACT

Ti-based coatings are utilized in a wide variety of applications, from biomedical implants to mechanical tools. Insight into initial stages of processes triggered by gas exposure and temperature change in the near-surface region of such coatings is essential for the understanding of their macroscopic behavior. We present an *in situ* time-of-flight low-energy ion scattering (ToF-LEIS) approach for the non-destructive and depth-resolved study of composition and morphology of the immediate surface region with sub-nm resolution. Ti-based coatings, with increasing compositional complexity, starting from *in situ* grown Ti, followed by *ex situ* grown Ti, TiN, and (Ti,Al)N, are studied concerning effects of exposure to oxygen and elevated temperatures. On the clean *in situ* deposited Ti surface, a 1.9 nm thick oxide layer is observed after exposure to 4000 Langmuir oxygen at room temperature. In contrast, for *ex situ* grown samples, an oxidic surface layer not removable by surface ion sputtering is found to limit effects of further oxygen exposure. TiN does not show significant changes when exposed to oxygen at 370 °C. For (Ti,Al)N, a nm-thick Al-rich surface layer is observed at annealing temperatures above 600 °C, both in ultra-high vacuum and in 1.0×10^{-3} Pa of oxygen.

1. Introduction

Titanium is a versatile transition metal featuring low density, high strength, low toxicity, high affinity for living tissue, and high resistance to corrosion in, e.g., seawater, aqua regia, and chlorine. These properties make titanium interesting for use in applications where thin films can be employed to functionalize or enhance the structural integrity of surfaces of otherwise lower-cost bulk materials such as steels. Examples of the use of pure titanium coatings can be found in biomedical applications, like Mg bone implants, where Ti-coatings improve corrosion resistance [1], and diamond tools, like diamond grits, where Ti-coatings increase the tool lifetime significantly [2]. Additionally, Ti coatings are used in vacuum applications for titanium sublimation pumps [3] and as non-evaporable getter (NEG) strips [4]. Titanium nitride (TiN) features high mechanical hardness, prompting its widespread use as a protective and wear-resistant coating [5]. Another area of broad application for TiN thin films is found in thin film electronics, where TiN films are used as diffusion barriers, gate electrodes, and interconnects [6–10]. The mechanical properties of TiN are exceeded by metastable titanium aluminum nitride ((Ti,Al)N) protective thin films, which significantly increase the wear resistance of steel or cemented carbide cutting tools [11,12]. Whereas Ti films readily oxidize at temperatures of 80 °C [13] and TiN shows oxidation from 550 °C, the onset of oxidation of $(Ti_{0.5}Al_{0.5})N$ is > 700 °C [11]. Additionally, while titanium shows a hexagonally close packed (hcp) structure, both TiN and (Ti,Al)N exhibit a face-centered cubic (fcc) crystal structure (NaCl prototype, space group $Fm\bar{3}m$). Comparing TiN and (Ti,Al)N, it has been shown that the addition of aluminum causes the formation of an Al_2O_3-containing oxide scale upon annealing in air [14]. Recent systematic studies revealed that the oxidation of (Ti,Al)N coatings is governed by the annealing temperature and the aluminum content [15,16].

However, the above-discussed studies were concerned with oxide scales at the order of several tens to hundreds of nanometers. Since the coated components are often stored and utilized in atmosphere, the initial interaction of the film surface with an oxygen-containing atmosphere at room and elevated temperatures is of interest. Usually, the

* Corresponding author.
E-mail address: philipp.wolf@physics.uu.se (P.M. Wolf).

https://doi.org/10.1016/j.apsusc.2023.158076
Received 19 April 2023; Received in revised form 3 July 2023; Accepted 18 July 2023
Available online 20 July 2023

overall coating composition does not represent the surface composition as X-ray photoelectron spectroscopy (XPS) data revealed oxygen concentrations of 40 to 60 at.% for (Ti,Al)N and (Ti,Al)(O,N) coatings and surface oxidation was suggested to occur due to residual gas incorporation or atmosphere exposure [17]. It has also been demonstrated that the venting temperature substantially influences the composition and thickness of such surface oxides [18]. In addition, the chemisorption of oxygen on (Ti,Al)N surfaces has been studied with XPS: Fresh surfaces were obtained using Ar sputter cleaning, and oxidation was carried out *in situ* with an oxygen partial pressure of 0.9×10^{-6} Pa [19]. Upon oxygen exposure, Ti_2O_3-like bonding and Ti vacancy formation were observed, while the interaction of aluminum with oxygen was not as pronounced [19]. The dissociative adsorption of O_2 on Ti sites can be understood by an increased Ti–O bond strength relative to Al–O bonds as predicted by *ab initio* molecular dynamics calculations [20]. However, surface processes have not been studied for (Ti,Al)N at thermal decomposition temperatures when, e.g., spinodal decomposition into isostructural TiN- and AlN-rich domains [21] is activated.

Hence, tools sensitive to the composition and morphology of near-surface regions and ultra-thin films are of increasing importance. Here, we present an *in situ* time-of-flight low-energy ion scattering (ToF-LEIS) characterization of the initial oxidation stages of surfaces of titanium-based thin films.

Sharing many of the fundamental physical concepts with the more common Rutherford backscattering spectrometry (RBS), ToF-LEIS, using ion energies in the range of 0.5–10 keV, yields depth-resolved information on the near-surface sample composition and, utilizing shadowing and blocking effects, the near-surface structure of samples [22–27]. Just as RBS, ToF-LEIS can be considered non-destructive because the primary ion current of about 4×10^7 mm^{-2} s^{-1} is significantly lower than the number of surface atoms exposed, even at a typical measurement time of 600 s. An example of the capabilities of ToF-LEIS is the quantitative *in situ* analysis of the initial stages of growth of heavy metallic species on light substrates, like Au on B [25]. Here, ToF-LEIS, which can analyze both ions and neutrals separately with a post-acceleration stage, was demonstrated to be capable of determining the growth mode as cluster growth and of measuring the aspect ratios of the clusters. Making use of crystal symmetries, monolayer resolution has been demonstrated to be achievable for CuAu-superstructures [26]. Finally, a recent study on phase transitions in ultra-thin nickel silicide films illustrated the potential of ToF-LEIS for *in situ* characterizations of ultra-thin films of transition metal compounds [27].

To characterize the initial oxidation stages of surfaces of titanium-based thin films, we investigate the near-surface composition under exposure to oxygen and at elevated temperatures for two Ti films, one of the two deposited *in situ*, then study a TiN film before arriving at the (Ti,Al)N samples. By starting with simpler systems and advancing towards more compositionally complex and oxidation-resistant systems, a more profound understanding of both the Ti-based surfaces and the data obtained by ToF-LEIS and corresponding Monte-Carlo simulations is reached. As a result, our data show the formation of an aluminum-rich surface layer at elevated temperatures for (Ti,Al)N samples. The formation of this aluminum-rich surface layer indicates that the onset of the formation of the double-layer oxide scale is supported by Al mobility. Our data further corroborate the established increase in oxidation resistance for the TiN and (Ti,Al)N samples as compared to pure Ti samples.

2. Experimental methods

Samples were grown both *in situ*, using e$^-$–beam evaporation, and *ex situ*, using sputter deposition.

The *in situ* deposition of Ti on a Si(1 0 0) substrate was performed by e$^-$-beam evaporation, using a UHV Evaporator 3T by Omicron, which was operated at a filament current of 2.25 A and a high voltage of 1 kV at a maximum pressure of 4.1×10^{-8} Pa. With a nominal deposition rate of 0.16 nm min^{-1} and a deposition time of 57 min 30 sec, a film thickness of 9 nm was expected. The amount of deposited Ti was determined to be 49×10^{15} atoms cm^{-2}, corresponding to a thickness of 8.6 nm assuming a density of 4.52 g cm^{-3}, by an *ex situ* RBS measurement using a 2 MeV He^+ beam at the 5 MV pelletron accelerator at the Tandem Laboratory [28]. The 5 MV pelletron accelerator was further used to perform time-of-flight elastic recoil detection analysis (ToF–ERDA) using 36 MeV and 44 MeV iodine ions. ToF-ERDA measurements were used to determine the native oxygen content in the *ex situ* deposited Ti, TiN, and (Ti,Al)N films, as well as possible changes in the bulk of the films due to the exposure to oxygen at elevated temperatures. The ToF-ERDA measurements were not performed *in situ* and not directly after the *in situ* measurements, which can influence the results in the region close to the surfaces of the samples.

High-power pulsed magnetron sputtering (HPPMS) [29] was carried out in an industrial CemeCon CC800/9 deposition system. *Ex situ* grown Ti and TiN films were deposited with a rectangular Ti target (grade 2, purity > 99 wt.%) with dimensions of $50 \times 8.8 \times 1$ cm, and MgO(1 0 0), as well as Si(0 0 1) substrates, were placed at a target-to-substrate distance of 10 cm. The substrates were heated to 380 °C, and the base pressure at the end of the heating cycle was $< 3 \times 10^{-4}$ Pa. For Ti films, an Ar flow of 200 sccm was used, resulting in a pressure of 0.37 Pa, and for TiN, an N_2 flow of 30 sccm was added, corresponding to a total deposition pressure of 0.43 Pa. One Melec SIPP2000USB-16–500-5 power supply was used, and the pulsing scheme was identical for the growth of Ti as well as TiN with 1.5 kW time-averaged power, 50 μs pulse on-time and 1950 μs pulse off-time. The peak target power and peak target current densities were 280 W cm^{-2} and 0.4 A cm^{-2} as well as 360 W cm^{-2} and 0.5 A cm^{-2} for Ti as well as TiN depositions, respectively. The plasma was stopped after 56 min for Ti and 160 min for TiN, resulting in a thickness of 2 μm. The venting temperature was < 100 °C in order to minimize surface oxidation [18].

In case of (Ti,Al)N, a hybrid setup was used [30], and differences to the details provided above are described in the following. Besides the Ti target, an Al target (>99.9 wt.% purity) was placed in a co-sputtering geometry: the target-to-substrate distance was 16 cm, and the angle between target and substrate normal was ~ 28°. The MgO(1 0 0) substrates were heated to 500 °C, and the Ar and N_2 flows were 160 and 80 sccm, respectively, resulting in a deposition pressure of 0.44 Pa. The Ti target was DC magnetron-sputtered with a 10 kW ADL GX 100/1000 power supply, and two Melec SIPP2000USB-16–500-5 power supplies were employed for the Al target as well as the substrate bias. The DC power at the Ti target was 2.35 kW, and a time-averaged power of 2.5 kW was used for the Al target, which was operated with HPPMS. The peak target power and peak target current densities were 440 W cm^{-2} and 0.6 A cm^{-2}, respectively. A pulsed substrate bias of −300 V with a pulse length of 70 μs and a delay of 30 μs with respect to the pulse onset at the Al target was employed in order to separate the film-forming metallic species in time and energy domains [30]. The (Ti,Al)N deposition was carried out for 120 min, and a thickness of 3 μm was obtained.

The phase formation of *ex situ* grown films was studied with X-ray diffraction (XRD) using a Siemens D5000 system in Bragg-Brentano geometry. Voltage and current of the X-ray tube with Cu Kα radiation were 40 kV and 40 mA, respectively. A 2θ range of 20 to 80° was scanned with 0.5° step size, and 4 s dwell time.

All sample surfaces were analyzed in the ACOLISSA setup, consisting of a ToF-LEIS scattering chamber and a connected preparation chamber allowing for *in situ* analysis of the samples. The preparation chamber, housing the UHV Evaporator 3T used for the deposition of the Ti film, further includes setups for Auger electron spectroscopy (AES), low-energy electron diffraction (LEED), and ion sputtering. In the preparation chamber, samples can additionally be subjected to different gases. Exposure of samples to elevated temperatures is possible both in the preparation chamber and the scattering chamber. More detailed descriptions of the ACOLISSA setup are given by Draxler *et al.* [31] as well as by Ström and Primetzhofer [28].

The *ex situ* deposited samples were cleaned before the exposure to oxygen and elevated temperatures by ion sputtering using a 3 keV Ar^+ beam to remove potential surface impurities. The effect of the ion sputtering was assessed by AES measurements performed before and after the sputter runs. The cleaning process was continued until no further reduction in the oxygen content was visible, and the carbon surface contaminations were removed entirely.

Samples were exposed to elevated temperatures using a heating filament and by additionally applying a potential difference between filament and sample, leading to electron bombardment. Annealing temperatures were measured employing an optical pyrometer.

The samples were exposed to oxygen *in situ* by introducing 1.0×10^{-3} Pa of oxygen for 9 min or 1.0×10^{-4} Pa for 90 min into the preparation chamber, corresponding to a surface exposure of 4000 Langmuir. The lower oxygen pressure was chosen at elevated sample temperatures for the (Ti,Al)N and for the TiN sample to avoid damaging the filament used for heating the sample, while the Ti samples were exposed to the higher oxygen pressure. In cases in which the sample was exposed to an elevated temperature as well as oxygen, the oxygen was introduced into the chamber as soon as the sample reached the target temperature. The base pressure before the introduction of oxygen was on the order of 10^{-8} Pa in case of the sample not being exposed to elevated temperatures and on the order of 10^{-6} Pa for samples at elevated temperatures.

ToF-LEIS measurements were conducted *in situ*, before and after each exposure to oxygen. All presented ToF–LEIS measurements were performed using a He^+ beam at a scattering angle of 129°, an acceptance angle of 0.29°, an incident angle of 0°, and an exit angle of 51° both regarding the samples surface normal. ToF-LEIS spectra recorded after exposure to oxygen and high temperatures are normalized to the multiple scattering backgrounds of the spectra recorded before exposure to oxygen and high temperatures for easier comparability.

Simulations using the TRBS (TRIM for Rutherford backscattering) code [32], based on the Monte-Carlo code TRIM (Transport of Ions in Matter) [33], were performed to interpret the ToF-LEIS results. To increase the speed of simulations, the TRBS code exploits azimuthal symmetry under normal incidence and considers only large angle scattering events explicitly. At the same time, nuclear and electronic energy losses are calculated globally, enabling the time-efficient simulation of backscattering spectra for which millions of ion histories must be calculated. The stopping power data used in these simulations for compounds are taken from the stopping and range of ions in matter (SRIM) data [34]. Screening and scattering potentials were simulated according to the Ziegler-Biersack-Littmark (ZBL) model [35]. In the case of titanium, the stopping power was extrapolated from data obtained from measurements performed on the *in situ* grown titanium at helium beam energies of 4, 6, 8, and 10 keV. The stopping power for aluminum was extrapolated from the experimental data published in Ref. [36]. All TRBS simulations were run with 200 million projectiles. For the simulations with 6 keV helium projectiles, a cutoff angle of 9.2° was used, while a cutoff angle of 8.0° was applied for 2 keV helium projectiles. The results of the TRBS simulations are convoluted with a Gaussian distribution with an expectation value proportional to $E^{3/2}$ to account for the finite and energy-dependent detector resolution of the ToF-LEIS setup.

In addition to ToF-LEIS, AES was performed before and after each exposure to oxygen and elevated temperatures. All AES measurements were performed using a PHI 10–155 AES system. Compositions were calculated based on the peak heights observed in the AES spectra and the corresponding sensitivity factors as described by Davis *et al.* [37].

The transmission electron microscopy (TEM) images were taken using a FEI Titan Themis 200 TEM system at the acceleration voltage of 200 kV. The images were captured with the Ceta CMOS camera (Thermo Fisher Scientific). Lamellae for TEM were extracted from the samples using the focused ion beam (FIB) method with *in situ* lift out employing a FEI DualBeam FIB/SEM235 setup. Prior to the FIB process, protective Au/Pd and Pt layers were deposited on the sample surface.

A comparison of depth resolutions and probing depths of the techniques used in this work is summarized in Table 1.

3. Results and discussion

First, we present the *in situ* grown titanium sample, serving as a reference point for the *ex situ* samples. The AES measurement performed before the exposure to oxygen, included in Fig. 1a, shows a composition of 76 % titanium and 24 % oxygen. In the ToF–LEIS measurement (Fig. 2a), recorded before exposure to oxygen, a clean Ti signal is visible. The AES and the ToF–LEIS spectra change significantly due to the 9 min exposure to 1.0×10^{-3} Pa oxygen. In the AES spectra, a significant increase in the size of the oxygen KLL peak is observed, and the composition derived from the spectra changes to 43 % titanium and 57 % oxygen, which could indicate the formation of a near-surface Ti_2O_3 layer. Alternatively, a gradient in oxygen content with more oxygen, likely TiO_2, at the surface and an oxygen decrease with increasing depth is possible. Such an oxygen gradient would not be visible in AES, which is not depth resolved. Another effect observed in the AES spectrum is the increase of the Ti peak at 387 eV compared to the size of the Ti peak at 418 eV. It is known that this change in the relative size of the two peaks can be related to the oxidation state of titanium and that an increase of the 387 eV peak relative to the 418 eV peak indicates a higher amount of oxygen. The reason for this relative change in peak size is that only the Ti peak at 418 eV, the LMV peak, includes valence electrons involved in the oxidation of the sample [41,42]. Calculating the ratio between the height of the two peaks, Ti(418 eV)/Ti(387 eV), yields a value of 0.9 for the measurement before and a value of 0.6 for the measurement taken after the exposure to oxygen. According to Rao *et al.* [41], a value of 0.6 corresponds roughly to a TiO oxidation state, which is close to the compositions calculated from the peak heights.

Not only the AES spectrum but also the ToF-LEIS spectrum, shown in Fig. 2a, changes significantly due to the exposure of the sample to oxygen. The yield close to the kinematic energy of helium ions scattered from titanium decreases, while it stays unchanged at lower energies, with a step appearing at an energy of roughly 1.3 keV. This decrease in yield related to titanium indicates a decrease in the number of titanium atoms present in the surface area, one of two effects of oxidation observable in ToF-LEIS spectra. The other effect would be the appearance of a peak at the energy corresponding to the kinematic energy of a primary ion scattered from oxygen. The second option is explained by an enlarged probability of the incoming ions scattering on oxygen atoms, increasing the number of ions reaching the detector with the corresponding energy. An increased probability for the incoming ions to scatter on oxygen atoms consequently leads to a decreased probability for the incoming ions to scatter on the heavier elements because their relative number at the surface is decreased, which results in a reduction in yield from scattering from the heavier elements at the surface thus explaining the effect observed for the *in situ* titanium sample. The appearance of an oxygen peak is, in most cases, only visible for a substantial increase in the amount of oxygen, mainly due to the low scattering cross section of oxygen; thus, commonly, oxygen is evidenced indirectly.

To thus further confirm that the decrease in yield is caused by oxidation of the surface, Monte-Carlo simulations using the TRBS code were performed. The simulations, shown in Fig. 3a, assume the formation of a surface oxide with TiO_2 composition. A good fit of the experimental data obtained from the oxidized sample is achieved by assuming

Table 1
Depth resolutions and probing depths of the methods employed in this study.

Method	Depth resolution	Probing depth	Ref.
ToF-LEIS	< 1 nm	≈ 10 nm	[38]
AES	–	≈ 1 nm	[37,39]
ToF-ERDA	> 10 nm	≈ 400 nm	[40]

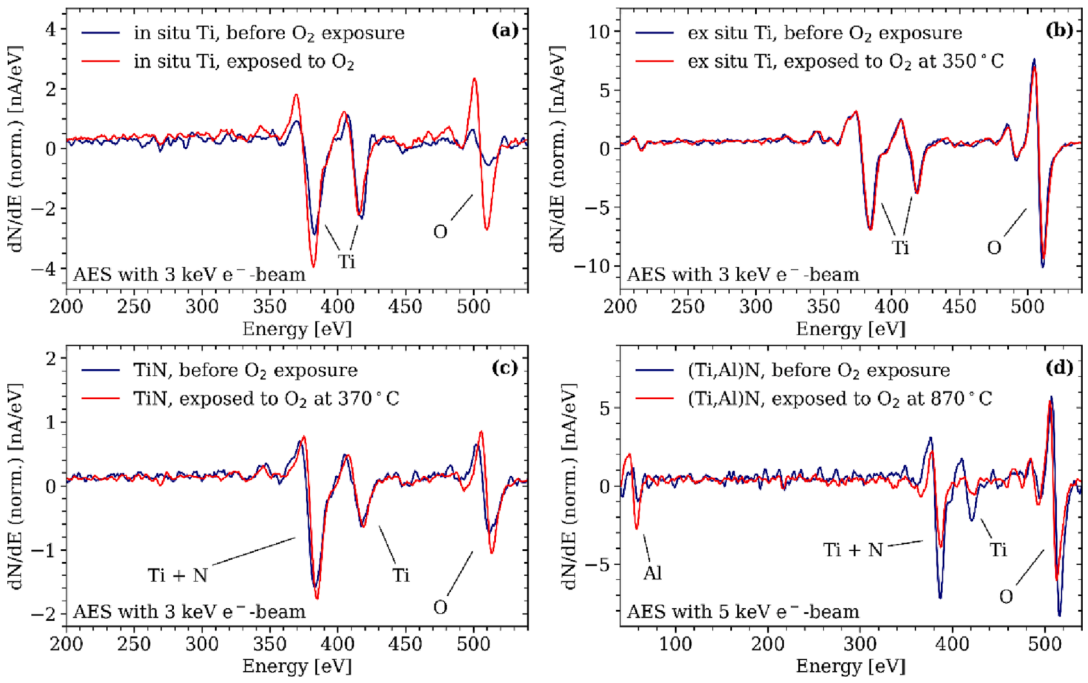

Fig. 1. AES measurements performed before (blue) and after annealing and exposure to oxygen (red) using a 3 keV e$^-$-beam for (a) *in situ* Ti, (b) *ex situ* Ti, and (c) TiN, as well as (d) a 5 keV e$^-$-beam for (Ti,Al)N. Peaks are marked with the corresponding elements. The spectra for (Ti,Al)N (d) are normalized to the sample current recorded during the measurement while the spectra for *in situ* Ti (a), *ex situ* Ti (b), and TiN(c) are normalized to the height of the titanium LMV peak at 418 eV.

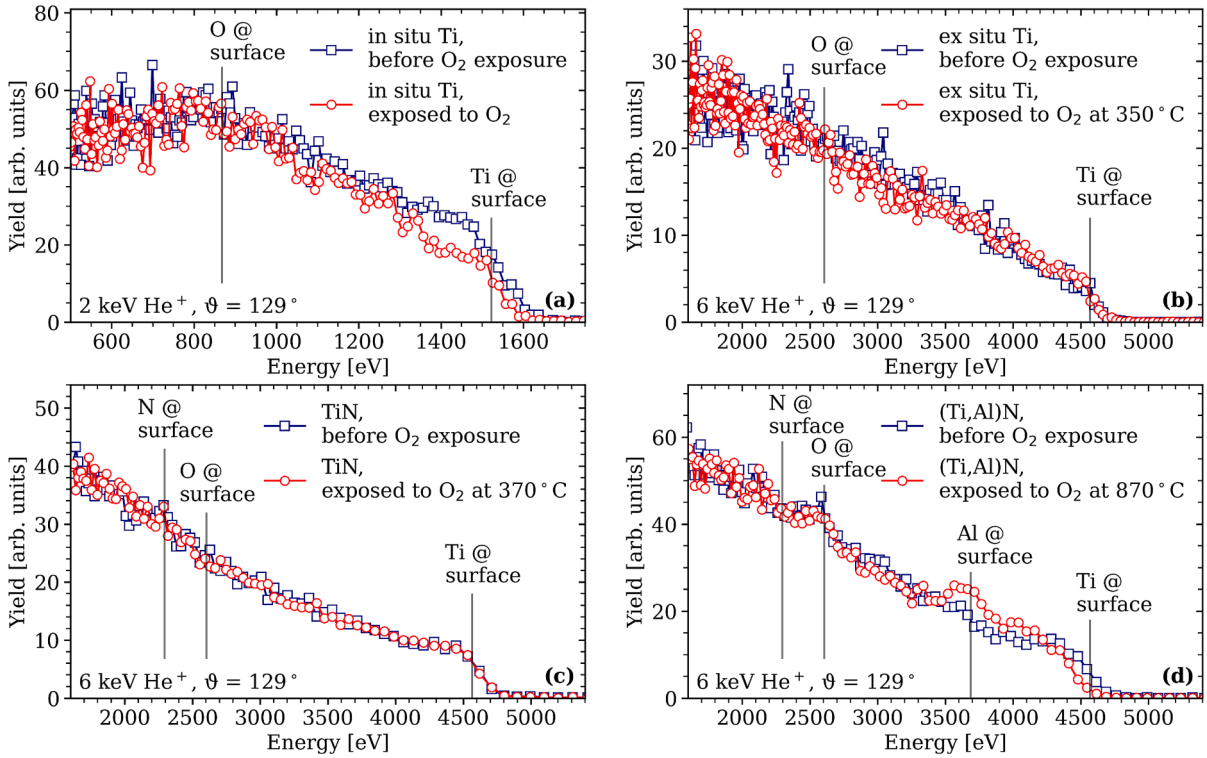

Fig. 2. ToF-LEIS spectra recorded before the exposure to oxygen (blue squares) and after the exposure to oxygen (red circles) using 2 keV He$^+$ ions for (a) the *in situ* deposited Ti as well as using 6 keV He$^+$ ions for (b) *ex situ* Ti, annealed to 350 °C during oxygen exposure, (c) TiN, annealed to 370 °C during oxygen exposure, and (d) (Ti,Al)N, annealed to 870 °C during oxygen exposure. ToF-LEIS spectra recorded after exposure to oxygen and high temperatures are normalized to the multiple scattering backgrounds of the spectra recorded before exposure to oxygen and high temperatures.

a TiO_2 layer thickness of $(18.36 \pm 3.66) \times 10^{15}$ at. cm^{-2}, equivalent to (1.91 ± 0.38) nm with a density of 4.25 g cm^3, on the surface of the titanium sample. TRBS simulations depicting the uncertainty limits for the TiO_2 thickness are included in the figure as thinner purple lines. For the ToF-LEIS spectrum recorded before exposure to oxygen, the simulation of a clean Ti surface results in a good agreement between

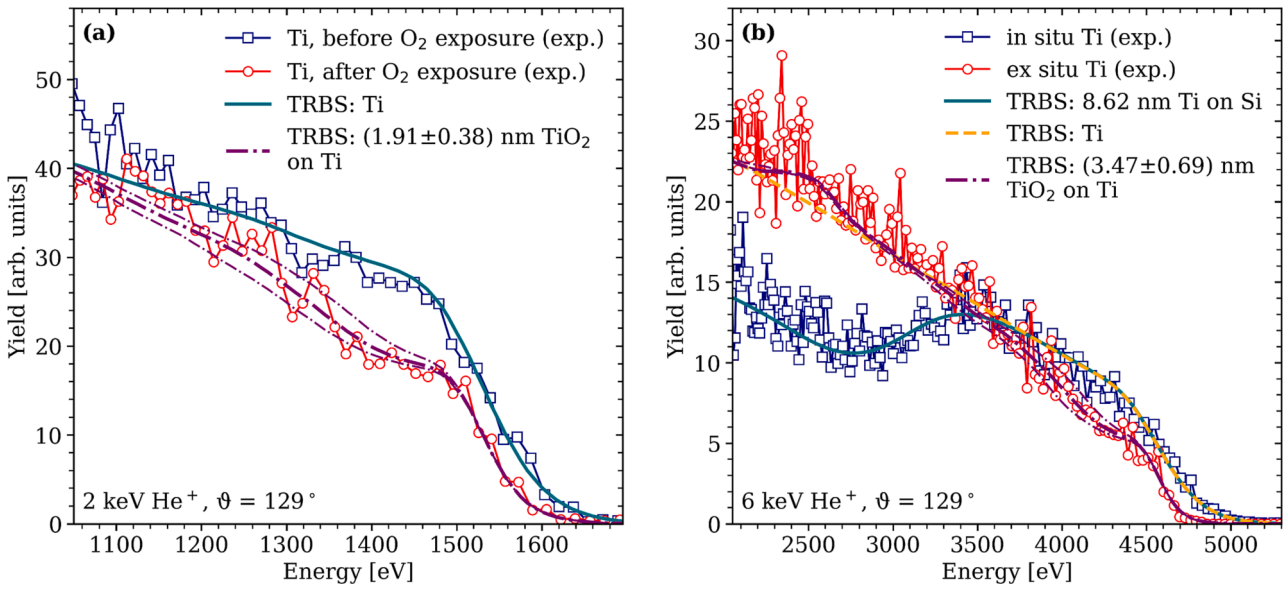

Fig. 3. (a) ToF-LEIS spectra of the *in situ* Ti sample before and after exposure to oxygen utilizing a 2 keV He^+ beam fitted by TRBS simulations of a clean Ti sample and a Ti sample with a TiO_2 surface layer. (b) ToF-LEIS spectra of the *in situ* grown Ti sample and the *ex situ* grown Ti sample utilizing a 6 keV He^+ beam as well as TRBS simulations of clean Ti samples and a Ti sample with an oxidized surface. TRBS simulations depicting the upper and lower uncertainty limit of the TiO_2 thickness are included as thinner purple lines in both figures.

simulation and experiment. While a larger film thickness than the here employed 9 nm would be preferable for comparison with industrially relevant coatings, the film thickness is shown to be large enough to study the often not considered initial stages of oxidation with the ToF-LEIS method and with AES.

The phase formation of the *ex situ* grown Ti, TiN, and (Ti,Al)N films is presented in Fig. 4. All films are single-phase, and the diffraction peaks of the Ti and TiN films are consistent with the corresponding reference lines (Fig. 4a,b). In case of (Ti,Al)N, a metastable cubic solid solution is formed.

In contrast to the *in situ* grown Ti sample, the *ex situ* grown Ti, TiN, and (Ti,Al)N samples all show an oxidized surface, visible both in AES and ToF-ERDA measurements, already before being exposed to oxygen in the ACOLISSA setup. Due to the exposure to the atmosphere during transport, oxidation of the surface has to be expected. The results of the ToF-ERDA measurements are presented in Figure S1 and Table S1 of the supplementary material. In the case of the as-deposited *ex situ* grown Ti sample, the ToF-ERDA measurement confirms surface oxidation up to a depth of approximately 150 × 10^{15} atoms cm^{-2}, or about 26 nm, assuming a density of 4.52 g cm^{-3}. Since this is the density of bulk Ti and ToF-ERDA shows the oxide layer to have a gradient with a decrease of oxygen with depth, the conversion from thin film thickness units to nm can only be an estimation. The average amount of oxygen detected in the first 100 × 10^{15} atoms cm^{-2} (ca. 18 nm) of the sample is (15.4 ± 1.4) %, while the oxygen amount in the bulk of the sample is (0.3 ± 0.1) %. Additionally, small amounts of carbon (1.3 ± 0.6) % and nitrogen (1.4 ± 0.6) % are detected in the surface region but not in the bulk. For the as-deposited TiN sample, a similar picture emerges, with ToF-ERDA showing surface oxidation up to a depth of approximately 100 × 10^{15} atoms cm^{-2}, which corresponds to about 20 nm assuming a density of 5.21 g cm^{-3}. The oxygen content in the first 100 × 10^{15} atoms cm^{-2} is (6.7 ± 0.8) %, while the nitrogen content is reduced to (34.0 ± 2.1) %, and the titanium content is (59.0 ± 2.0) %. In the bulk of the sample, almost no oxygen is present with (0.3 ± 0.1) %, while the nitrogen and titanium contents are as expected for TiN, with (50.2 ± 0.9) % nitrogen and (49.4 ± 0.8) % titanium. Additionally, a small amount of hydrogen, with a concentration of around 0.2 %, is detected. For the as-deposited (Ti,Al)N sample, the ToF-ERDA measurement shows surface oxidation to a depth of approximately 200 × 10^{15} atoms cm^{-2}, corresponding to 37 nm, assuming a density of 4.69 g cm^{-3}. The oxygen content within the first 100 × 10^{15} atoms cm^{-2} (ca. 18 nm) is (11.0 ± 0.7) %, while the nitrogen is reduced to (40.9 ± 1.3) % from a bulk concentration of (51.4 ± 0.7) %. Oxygen is almost absent from the bulk of the sample, with a concentration of (0.6 ± 0.1) %. Both titanium and aluminum show an essentially constant concentration throughout the sample, with a bulk concentration of (20.9 ± 0.4) % for titanium and (26.7 ± 0.5) % for aluminum. Additionally, small amounts of hydrogen and argon, stemming from the sputter deposition of the film, can be seen in the sample. Both the hydrogen and the argon concentration are significantly lower than 1 % in the bulk of the sample. For all *ex situ* synthesized samples, it thus can be concluded that they feature high-purity crystallites with contaminants likely being concentrated along grain boundaries. Oxygen diffusion along grain boundaries has been observed before in metallic [43] as well as carbide [44] and nitride [45] thin films. Thus, the grain boundaries are also expected to be the favored pathway for oxygen diffusion during oxygen exposure of the here studied systems.

The *ex situ* grown samples were sputter cleaned using argon ions in the preparation chamber to remove the oxidized surface layer. After multiple hours of sputter cleaning, the amount of oxygen did not reduce further, leaving a significant percentage of oxygen at the sample surface, visible through the oxygen peak at around 500 eV seen in the AES spectra of all *ex situ* grown samples recorded before the deliberate exposure to oxygen (Fig. 1b-d). The remaining oxygen possibly results from a reduced sputter yield of oxygen as compared to other elements in the film leading to an equilibrium of the surface composition. Alternatively, residual H_2O or O_2, might oxidize the surface during Ar sputtering or AES. Such an oxidation by residual gases has not been observed for other samples in the setup though.

For the *ex situ* grown Ti sample, the oxygen content observed in the AES measurements stayed unchanged after multiple cycles of sputtering at roughly 72 %, the level also observed in the AES measurement performed before annealing and concomitant oxygen exposure shown in Fig. 1b. The composition indicated by the AES measurement fits that of a titanium dioxide layer at the surface. Exposing the sample for 9 min to 1.0 × 10^{-3} Pa oxygen to achieve the same surface exposure as for (Ti,Al)N and TiN, at a temperature of 350 °C, did consequently not increase the amount of oxygen at the surface significantly, visible by the unchanged size of the oxygen peak in the AES measurement (Fig. 1b), from which an

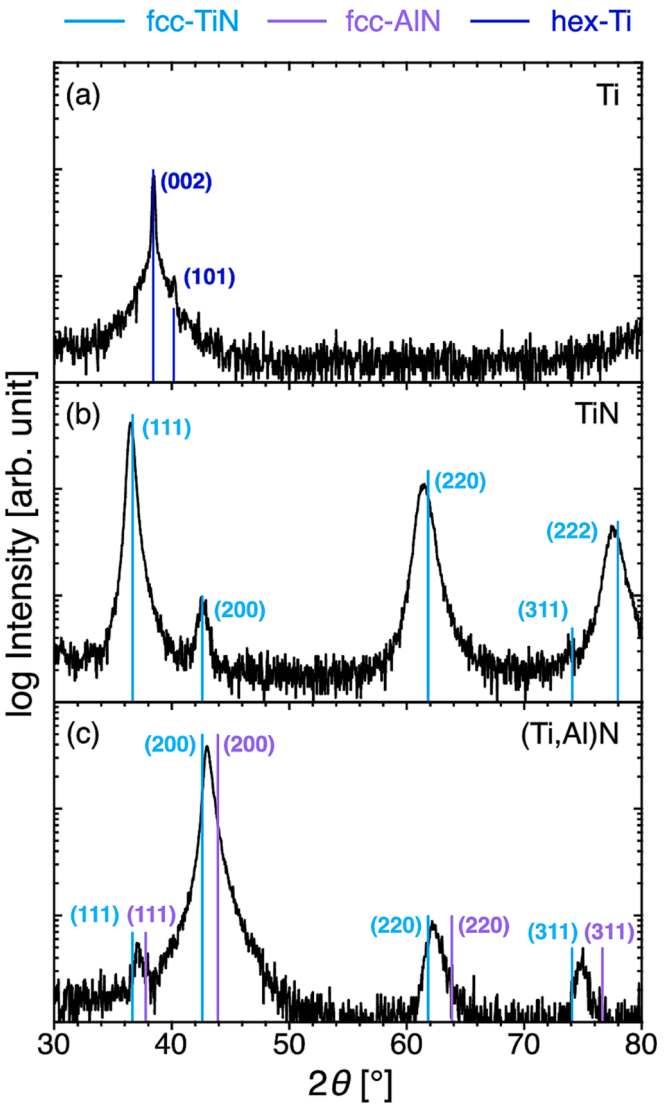

Fig. 4. X-ray diffractograms of (a) Ti, (b) TiN, and (c) (Ti,Al)N. Reference lines are taken from the International Centre for Diffraction Data (ICDD) and correspond to 00–044-1294 (blue) for hexagonal (hex-)Ti, 00–038-1420 (cyan) for fcc-TiN and 00–025-1495 (purple) for fcc-AlN.

oxygen content of about 70 % follows. An elevated temperature of 350 °C was chosen for this experiment since the already present surface oxide made a further oxidation at room temperature unlikely. As in the AES spectra, the ToF-LEIS spectra, depicted in Fig. 2b, do not show significant differences. A small visible difference is a slight reduction in yield at an energy of roughly 3.25 keV. This decrease might indicate a reduction of the fraction of titanium at a deeper level in the sample, which could be explained by an increased thickness of the surface oxide layer. Nevertheless, due to the small size of the change in the spectra, this increased oxide layer thickness cannot be asserted beyond all doubt. In the ToF–ERDA measurement, which is presented in the supplementary Figure S1b and Table S1, no change in composition is observed in the bulk region of the sample exposed to oxygen at an elevated temperature. The thickness of the surface oxide layer is approximately 200 $\times$ 10^{15} atoms cm^{-2}, up from about 150 $\times$ 10^{15} atoms cm^{-2} for the as-deposited sample (Figure S1a). The average oxygen content in the topmost 100 $\times$ 10^{15} atoms cm^{-2} increased by 19.4 percentage points to (33.2 $\pm$ 1.0) % compared to the ToF-ERDA measurement recorded before the annealing in an oxygen atmosphere. Since the ToF-ERDA measurement was performed *ex situ,* parts of the oxygen in the surface region might stem from exposure to atmospheric oxygen. The differences between the results of AES and ToF-LEIS on the one side and ToF-ERDA on the other can be explained by the different information depths and depth resolutions of the different methods.

As in the case of the *in situ* titanium sample, TRBS simulations were used to further analyze the ToF-LEIS spectra of the *ex situ* titanium sample. For this reason, an additional measurement using a 6 keV helium beam was performed on the as-deposited *in situ* titanium sample to compare it to the *ex situ* titanium sample. Both the ToF-LEIS spectra of the *in situ* titanium and of the *ex situ* titanium are presented together with TRBS simulations in Fig. 3b. In the case of the *in situ* grown titanium film, the thickness of only 49 $\times$ 10^{15} atoms cm^{-2} (ca. 8.6 nm) means that the information depth of the ToF-LEIS measurement at 6 keV is large enough to penetrate the titanium layer, resulting in the depicted titanium plateau and the yield corresponding to the silicon substrate appearing below roughly 2.5 keV. The ToF-LEIS spectrum of the *in situ* titanium sample agrees with the TRBS simulation of a clean 8.6 nm titanium layer on a silicon substrate.

In contrast, the *ex situ* sample shows an apparent deviation from the TRBS simulation of a clean titanium sample at energies above 3.5 keV. A better agreement between the ToF-LEIS spectra for *ex situ* titanium and the TRBS simulation is reached when a (33.36 $\pm$ 6.63) $\times$ 10^{15} at. cm^{-2} titanium oxide (TiO_2) layer, or (3.47 $\pm$ 0.69) nm again assuming ρ = 4.25 g cm^{-3}, is added to the sample surface (Fig. 3b). Thus, the ToF-LEIS measurement, together with the TRBS simulation, agrees with the AES results that indicate the presence of a persistent oxide layer on the *ex situ* titanium surface. Since SRIM data often deviates from experimental data at low ion energies, like the ones used here, the oxide thickness indicated by the TRBS simulation might not be accurate. However, it can serve as a well-founded assumption.

For TiN, the AES spectra (Fig. 1c) do not allow a determination of the complete surface composition due to the overlap of the titanium LMM line at 387 eV with the nitrogen KLL line at 379 eV, rendering the determination of the nitrogen amount impossible. Nevertheless, it is possible to determine the relative amounts of titanium, and oxygen, disregarding nitrogen. The observed ratio before the annealing to 370 °C and accompanying exposure to oxygen is 47 % titanium to 53 % oxygen, while it is 40 % titanium to 60 % oxygen afterward. Although the AES spectra show a slight increase in oxygen, this is not indicated by a change in the ToF-LEIS spectrum (Fig. 2c), which appears unchanged compared to the spectrum recorded before annealing and the concomitant oxidation. The experiment was conducted at the elevated temperature of 370 °C since the already present surface oxide made further oxidation at room temperature unlikely. A possible explanation for the lack of changes in the ToF-LEIS spectra is given by the similar mass of nitrogen and oxygen, the effect of which is a very similar kinematic factor for ions being scattered on nitrogen and oxygen. Additionally, as mentioned before, the scattering cross sections of oxygen and nitrogen are significantly lower than the scattering cross section of titanium. Based on the Ziegler-Biersack-Littmark potential, the differential scattering cross section of oxygen is 9.2 $\times$ 10^{-25} m^2 sr^{-1}, of nitrogen is 7.0 $\times$ 10^{-25} m^2 sr^{-1}, and of titanium is 5.1 $\times$ 10^{-24} m^2 sr^{-1} for 6 keV helium at a scattering angle of 129°. If the increased amount of oxygen close to the surface comes at the cost of a reduced amount of nitrogen, while the total amount of titanium atoms in the surface region stays unchanged, and oxygen and nitrogen contribute equally to the electronic energy loss, a difference in the ToF-LEIS spectra recorded before and after the annealing and oxidation would be minimal. While the ToF–LEIS spectra indicate no change, the ToF-ERDA measurements, included in supplementary Figure S1d and Table S1, show an increase of the oxygen content by 7.2 percentage points to (13.9 $\pm$ 1.4) % within the topmost 100 $\times$ 10^{15} atoms cm^{-2} ($\approx$20 nm) of the in oxygen annealed TiN sample. The composition in the bulk of the sample stays unchanged as compared to the as-deposited sample. While it is known that TiN oxidizes for higher temperatures and/or higher amounts of offered oxygen, we do not observe significant oxidation at the here-employed oxygen

pressures, which are orders of magnitude lower than in ambient air.

For (Ti,Al)N, again, the overlap between the nitrogen KLL and the titanium LMM line, as occurring in the case of TiN, limits the possibility of calculating compositions based on the AES data (Fig. 1d). Disregarding nitrogen, the peak height in the AES spectrum amounts to roughly 21 % of titanium, 20 % of aluminum, and 59 % of oxygen in the unannealed and not further oxidized sample. The ToF-LEIS spectrum (Fig. 2d) recorded before the annealing under oxygen exposure shows the titanium and the aluminum within the sample as distinct steps observable in the spectra. After the sample was annealed for 90 min at a temperature of 870 °C and an oxygen pressure of 1.0×10^{-4} Pa, two distinct changes appeared in the ToF-LEIS spectrum. The experiment was conducted at 870 °C, because it is known that the stability of (Ti,Al)N films decreases at these temperatures and spinodal decomposition occurs [21,46].

The first change is a shift of the front edge of the yield corresponding to titanium from an original position of approximately 4.6 keV to lower energies, and the second is the appearance of a peak at 3.7 keV, the energy corresponding to helium ions scattered on aluminum close to or at the surface of the sample. Both the shift of the titanium edge and the appearance of the aluminum peak reveal the formation of an aluminum-rich layer at the sample surface. The likely composition of this surface layer will be explored in more detail using Monte Carlo simulations. Again, the region of the spectrum corresponding to helium scattered on oxygen or nitrogen does not change significantly, thus indicating no large changes in the total oxygen and nitrogen content of the sample surface. The AES spectrum recorded after annealing under oxygen exposure supports these observations (Fig. 1d) and yields a composition, again excluding nitrogen, of 8 % titanium, 45 % aluminum, and 48 % oxygen. Thus, compared to titanium and aluminum, the percentage of oxygen even decreases during annealing under oxygen exposure. As ToF-LEIS, with its information depth of about 10 nm, and AES, with its sub-nm information depth, do not show an oxygen increase at the immediate surface area, a deeper look into the bulk of the sample using ToF–ERDA also does not show any increase in oxygen, nor any other significant composition change, compared to the measurement performed on a pristine twin sample. An analysis of the surface composition was impossible due to a thin platinum and palladium film deposited during the sample preparation for the TEM measurement, performed after the sample was exposed to elevated temperatures and oxygen in the ACOLISSA setup. The ToF-ERDA depth profile and the derived compositions are included in supplementary Figure S1f and Table S1.

The shift of the titanium edge is not only observed when the sample is exposed to oxygen during annealing, as the case for Fig. 2d, but also when the sample is annealed in an ultra-high vacuum. ToF-LEIS spectra recorded after sequential vacuum annealing steps of a (Ti,Al)N sample are presented in Fig. 5a. The spectra show that a significant shift of the titanium edge is observed at annealing temperatures above 600 °C, accompanied by the appearance and growth of a peak at ≈3.7 keV corresponding to 6 keV He^+ scattered from aluminum at ϑ=129°. The magnitude of the shift can be determined by fitting the titanium edge with an error function to determine the edge position, the results of which are displayed in Fig. 5b. These fits show that the titanium edge is shifted towards lower energies by (145 ± 33) eV after annealing the sample to 950 °C, compared to the original titanium edge position. The error bars depicted in Fig. 5b consist of the uncertainty given by the fitting of the experimental edges. Additional sources for uncertainties on the edge position include the channel width and the sample position (see Figure S4). Both the channel width and the sample position can be classified as systematic errors and hence have no influence on the trend observed in Fig. 5b. As in the case of the titanium edge shift, a quantification of the aluminum peak growth shows a significant change at temperatures above 600 °C with an increase in yield corresponding to aluminum at the surface. The yield in the aluminum peak calculated by integrating the energy spectrum from 3250 eV to 3686 eV and subtracting the yield observed at room temperature is shown in the supplementary Figure S3. The upper integration limit is the energy of a 6 keV helium ion scattered on aluminum at a scattering angle of 129°, while the lower limit is chosen to contain the whole aluminum peak within the integrated area as observed at the highest annealing temperature.

As mentioned before, the shift of the titanium edge, together with the appearance of the peak at the energy corresponding to 6 keV He^+ scattered on aluminum, shows the formation of an aluminum-rich surface layer. Fitting the ToF-LEIS spectra with TRBS yields further information on the thickness and composition of this aluminum-rich surface layer. Before simulating the spectrum of an annealed sample, the spectrum of an unannealed sample is simulated to serve as a starting point.

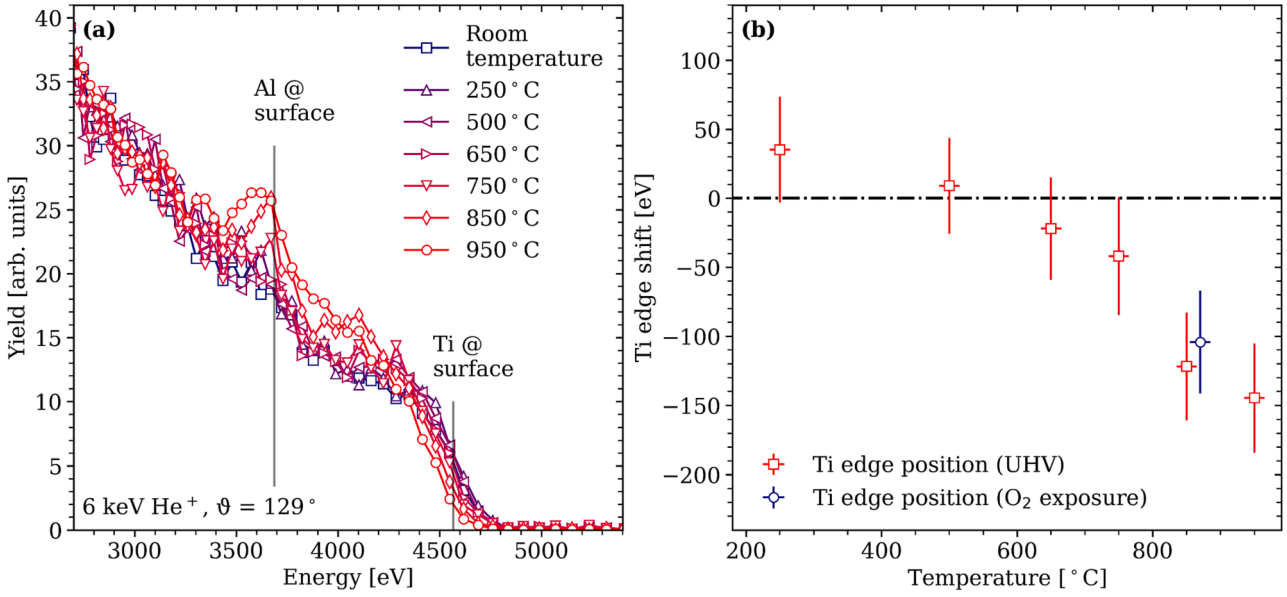

Fig. 5. (a) ToF-LEIS measurements utilizing a 6 keV He^+ beam showing spectra recorded after sequential annealing steps in an ultra-high vacuum of a (Ti,Al)N sample and (b) the shift of the position of the Ti surface edge in the ToF-LEIS spectra determined by fitting the edge with an error function. In (b) the shift of the Ti surface edge during the annealing in an ultra-high vacuum is represented by red squares, while the shift during annealing under oxygen exposure is depicted by a blue circle.

There are two sources of information on the composition of the unannealed sample. The first is the ToF-ERDA measurement which indicates a surface composition of 20.2 % titanium, 27.2 % aluminum, 11.0 % oxygen, 40.9 % nitrogen, and minimal amounts of hydrogen and argon. In contrast, the second source of information, which is the AES measurement, indicates roughly 21 % of titanium, 20 % of aluminum, and 59 % of oxygen, disregarding nitrogen, as mentioned before. The fact that the nitrogen content was disregarded in the AES composition does not significantly impact the TRBS simulations of the ToF-LEIS spectra, which are mostly shaped by the ratio of titanium to aluminum and in which the oxygen has very similar effects as the nitrogen would have. Using the ToF-ERDA composition in the TRBS simulation leads to an overestimation of the aluminum compared to the titanium. In contrast, a TRBS simulation based on the AES composition fits the ToF-LEIS spectra well, as seen in Fig. 6a. Due to its high surface sensitivity, it is not surprising that the ToF-LEIS spectrum is in better agreement with the composition derived from the AES measurement than the ToF-ERDA measurement. Consequently, the combined ToF-LEIS and AES data indicate that the surface of the (Ti,Al)N sample is aluminum depleted before the annealing of the sample, compared to the bulk composition derived from the ToF-ERDA data. These results are in agreement with the findings of Kunze *et al.* [19], who observed a larger interaction between titanium and oxygen than between aluminum and oxygen on the surface. One additional reason for the observed aluminum depletion at the surface could lie in the sample preparation, during which the surface was cleaned using 3 keV argon ions to sputter away surface impurities. If the aluminum is preferentially sputtered by argon ions, an aluminum depletion on the surface occurs. Such a preferential sputtering of aluminum is indicated by the empirical formula for sputtering yields published by Yamamura *et al.* [47,48], with sputtering yields of 2.5 atoms per ion for aluminum and 1.2 atoms per ion for titanium for the case of 3 keV argon ions at normal incidence.

Based on the TRBS simulation fitting the ToF-LEIS spectrum of the (Ti,Al)N sample before the annealing, simulations of the spectrum recorded after annealing to 950 °C can be performed. Here, we explored three options concerning the composition of the aluminum-rich layer formed on the sample surface. The first option is a pure aluminum layer, the second is an aluminum nitride (AlN) layer, and the third is an aluminum oxide (Al_2O_3) layer. To obtain the shift of the titanium edge observed in the experiment, a 1.60 nm aluminum layer (ρ = 2.70 g cm^{-3}), a 1.05 nm aluminum nitride layer (ρ = 3.26 g cm^{-3}), or a 0.90 nm Al_2O_3 layer (ρ = 3.99 g cm^{-3}) is necessary in the TRBS simulations, the results of which are presented in Fig. 6b. In all three cases, a reduction of the aluminum content in the subsurface layer by ten percentage points is necessary to reach a good agreement between simulation and experiment. While the simulations assuming an aluminum nitride or aluminum oxide surface layer underestimate the height of the aluminum peak, the simulation using pure aluminum fits the experiment well. However, it should be noted that even though the simulation of a pure aluminum surface layer shows the best agreement with the experimental data, it cannot be inferred that the surface layer consists only of aluminum. This inference is impossible since the TRBS simulations of aluminum nitride and aluminum oxide are performed using SRIM data for the electronic stopping power, which can be inaccurate at low ion energies. In order to obtain quantitative depth scales, reference stopping cross sections must be measured experimentally. Here, a lower electronic stopping power for the nitride and the oxide would mean that a thicker layer is needed to explain the shift of the titanium edge, which would also increase the size of the aluminum peak and lead to a better agreement with the experiment. Because we cannot exclude the possibility of the SRIM stopping power being larger than the actual stopping power, we cannot exclude the options of the surface layer being aluminum nitride or aluminum oxide. Additionally, a pure aluminum layer on the surface is thermodynamically unlikely, since the final annealing temperature of 950 °C significantly exceeds the melting point of aluminum at 660 °C. While the unknown electronic stopping power makes it impossible to report the exact thickness of the aluminum-rich surface layer, the total aluminum amount in the layer can be determined from the aluminum peak size. Here, the TRBS simulations indicate that the aluminum-rich surface layer contains approximately 9.6 × 10^{15} atoms cm^{-2} of aluminum. A ToF-ERDA depth profile of the in UHV conditions annealed (Ti,Al)N sample is included in supplementary Figure S2.

Additionally, in order to detect larger-scale changes in the sample due to the annealing and the exposure to oxygen, TEM images were taken of an as-deposited (Ti,Al)N film and the film exposed to oxygen at 870 °C. The TEM images included in Fig. 7 show no visible change due to the exposure to oxygen at 870 °C. In the case of the as-deposited sample, the Pd/Au and Pt protection layers, applied during the FIB preparation of the lamella for TEM, delaminated slightly from the film. Both samples show a polycrystalline structure, and no changes in this structure are observed between them.

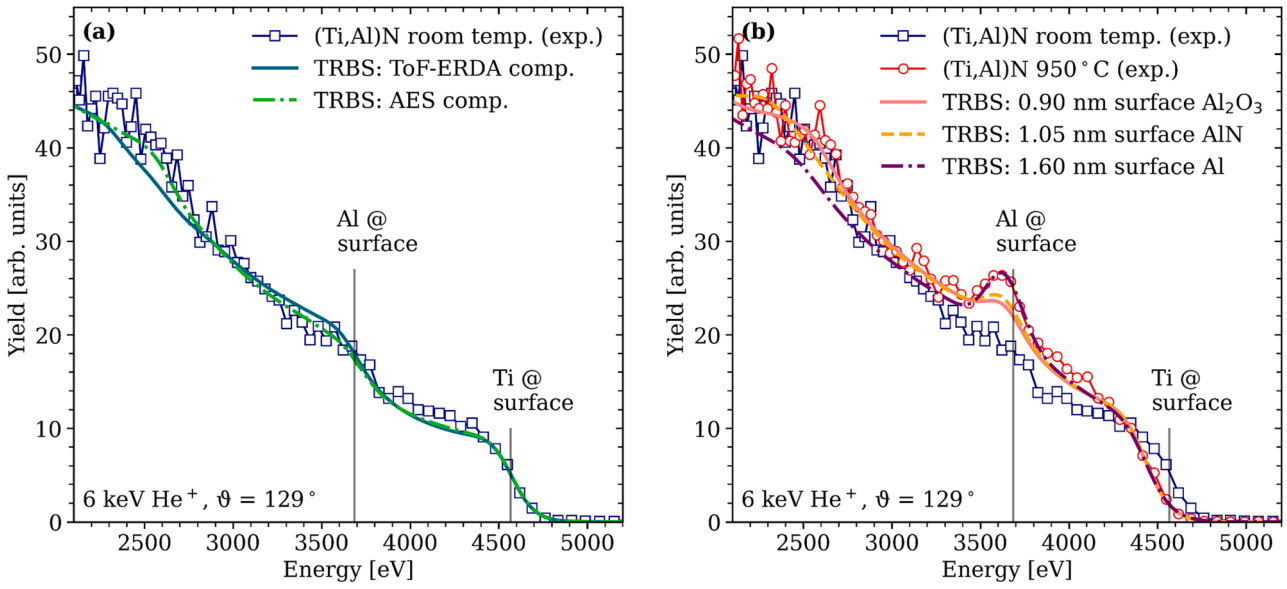

Fig. 6. (a) ToF-LEIS spectrum employing a 6 keV He^+ beam of a (Ti,Al)N sample, before annealing, fitted by TRBS simulations using compositions based on ToF-ERDA and AES. (b) ToF-LEIS, before and after annealing to 950 °C, fitted by TRBS simulations assuming an Al_2O_3, an AlN, and an Al surface layer.

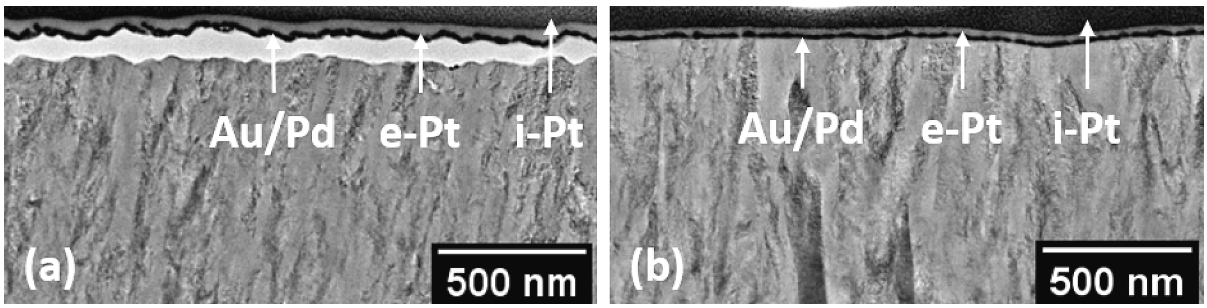

Fig. 7. TEM images of (a) a pristine (Ti,Al)N film and (b) the in oxygen annealed (Ti,Al)N film. The structure of both samples is equal, with a polycrystalline crystal structure. In the case of the pristine film, the Au/Pd and Pt protection layer delaminated from the surface of the sample.

The temperature-induced formation of an aluminum-rich surface layer can be understood by the comparatively low activation energy for Al displacement compared to Ti and N [49]. Moreover, the experimental observation of surface Al-enrichment can act as a precursor enabling the formation of a double-layer oxide scale with Al_2O_3 at the top during annealing in air [14].

4. Conclusions

The presented results show four main effects originating from the exposure of titanium and transition metal nitride surfaces to oxygen and elevated temperatures: (1) A clean titanium surface is shown to form a (1.91 ± 0.38) nm oxide layer already when exposed to oxygen amounts as low as 4000 Langmuir at room temperature. With TRBS simulations, it is possible to extract the thickness of this oxide layer from the recorded ToF-LEIS spectra. (2) Samples grown *ex situ* exhibit persistent oxidation of the surfaces, not removable through sputtering with argon ion doses of up to $\approx 9 \times 10^{16}$ atoms cm^{-2} in the case of Ti, $\approx 1 \times 10^{17}$ atoms cm^{-2} in the case of TiN, and $\approx 3 \times 10^{17}$ atoms cm^{-2} in the case of (Ti,Al)N. For the *ex situ* grown titanium film, the ToF-LEIS results, in combination with the TRBS simulations, determine the persistent oxidic surface layer to be (3.47 ± 0.69) nm thick. (3) *Ex situ* grown titanium and titanium nitride films do not experience a significant increase in oxygen at the surface, even when exposed to oxygen at temperatures of 350 °C and 370 °C, respectively. (4) While (Ti,Al)N films do not exhibit a detectable increase in oxygen in their surface region when exposed to oxygen at 870 °C, the formation of an aluminum-rich surface layer as confirmed by the ToF-LEIS measurements in connection with the TRBS simulations occurs. The formation of an aluminum-rich surface layer is not limited to the exposure of the (Ti,Al)N films to elevated temperatures and oxygen but is also observed when the sample is annealed at UHV conditions. This formation of an aluminum-rich surface layer, explained by the comparably low activation energy for the diffusion of aluminum, can be seen as the first step of the formation of the double-layer oxide scale with Al_2O_3 at the top which was observed during annealing in air by McIntyre *et al.* [14]. Finally, the here presented results show a qualitative agreement between ToF-LEIS and AES with quantitative differences stemming from the differing probing depths of the two methods. Thus, our findings exemplify the analytical power of ToF-LEIS in the depth-resolved characterization of surfaces and thin films, especially in connection with *in situ* sample preparation and modification.

CRediT authorship contribution statement

Philipp M. Wolf: Conceptualization, Data curation, Formal analysis, Investigation, Methodology, Project administration, Validation, Visualization, Writing - original draft, Writing - review & editing. **Deborah Neuß:** Data curation, Formal analysis, Investigation, Visualization, Writing - review & editing. **Tuan T. Tran:** Data curation, Formal analysis, Investigation, Supervision, Writing - review & editing. **Eduardo Pitthan:** Conceptualization, Formal analysis, Investigation, Supervision, Writing - review & editing. **Marcus Hans:** Conceptualization, Data curation, Formal analysis, Investigation, Methodology, Project administration, Supervision, Visualization, Writing - original draft, Writing - review & editing. **Jochen M. Schneider:** Conceptualization, Formal analysis, Funding acquisition, Methodology, Project administration, Supervision, Writing - review & editing. **Daniel Primetzhofer:** Conceptualization, Data curation, Formal analysis, Funding acquisition, Methodology, Project administration, Supervision, Visualization, Writing - review & editing.

Declaration of Competing Interest

The authors declare that they have no known competing financial interests or personal relationships that could have appeared to influence the work reported in this paper.

Data availability

Data will be made available on request.

Acknowledgments

Financial support from the Swedish Research Council (VR) (contract # 2020-04754_3) and support of the acceleration operation at Uppsala University by VR-RFI (contract # 2019-00191), the German Research Foundation (DFG) (contract # SCHN735/42-1) and the Swedish Foundation for Strategic Research (SSF) (contract # RIF14-0053) is gratefully acknowledged.

Appendix A. Supplementary data

Supplementary data to this article can be found online at https://doi.org/10.1016/j.apsusc.2023.158076.

References

[1] E. Zhang, L. Xu, K. Yang, Formation by ion plating of Ti-coating on pure Mg for biomedical applications, Scr. Mater. 53 (2005) 523–527, https://doi.org/10.1016/j.scriptamat.2005.05.009.
[2] Y.H. Wang, J.B. Zang, M.Z. Wang, Y. Guan, Y.Z. Zheng, Properties and applications of Ti-coated diamond grits, J. Mater. Process. Technol. 129 (2002) 369–372, https://doi.org/10.1016/S0924-0136(02)00661-1.
[3] D.J. Harra, Review of sticking coefficients and sorption capacities of gases on titanium films, J. Vac. Sci. Technol. 13 (1976) 471–474, https://doi.org/10.1116/1.568900.
[4] C. Benvenuti, P. Chiggiato, F. Cicoira, V. Ruzinov, Decreasing surface outgassing by thin film getter coatings, Vacuum 50 (1998) 57–63, https://doi.org/10.1016/S0042-207X(98)00017-7.
[5] E. Santecchia, A.M.S. Hamouda, F. Musharavati, E. Zalnezhad, M. Cabibbo, S. Spigarelli, Wear resistance investigation of titanium nitride-based coatings, Ceram. Int. 41 (2015) 10349–10379, https://doi.org/10.1016/j.ceramint.2015.04.152.
[6] M.Y. Kwak, D.H. Shin, T.W. Kang, K.N. Kim, Characteristics of TiN barrier layer against Cu diffusion, Thin Solid Films 339 (1999) 290–293, https://doi.org/10.1016/S0040-6090(98)01074-8.

[7] M. Moriyama, T. Kawazoe, M. Tanaka, M. Murakami, Correlation between microstructure and barrier properties of TiN thin films used Cu interconnects, Thin Solid Films 416 (2002) 136–144, https://doi.org/10.1016/S0040-6090(02)00602-8.

[8] L. Gao, J. Gstöttner, R. Emling, M. Balden, C.h. Linsmeier, A. Wiltner, W. Hansch, D. Schmitt-Landsiedel, Thermal stability of titanium nitride diffusion barrier films for advanced silver interconnects, Microelectron. Eng. 76 (2004) 76–81, https://doi.org/10.1016/j.mee.2004.07.020.

[9] M. Mühlbacher, A.S. Bochkarev, F. Mendez-Martin, B. Sartory, L. Chitu, M. N. Popov, P. Puschnig, J. Spitaler, H. Ding, N. Schalk, J. Lu, L. Hultman, C. Mitterer, Cu diffusion in single-crystal and polycrystalline TiN barrier layers: A high-resolution experimental study supported by first-principles calculations, J. Appl. Phys. 118 (2015) 085307, https://doi.org/10.1063/1.4929446.

[10] S. Englund, S. Grini, O. Donzel-Gargand, V. Paneta, V. Kosyak, D. Primetzhofer, J.J. S. Scragg, C. Platzer-Björkman, TiN interlayers with varied thickness in Cu $_2$ ZnSnS (e) $_4$ thin film solar cells: Effect on Na diffusion, Back contact stability, and Performance, Phys. Status Solidi A. 215 (2018) 1800491, https://doi.org/10.1002/pssa.201800491.

[11] W. Münz, Titanium aluminum nitride films: A new alternative to TiN coatings, Journal of Vacuum Science & Technology A. 4 (1986) 2717–2725, https://doi.org/10.1116/1.573713.

[12] O. Knotek, W. Münz, T. Leyendecker, Industrial deposition of binary, ternary, and quaternary nitrides of titanium, zirconium, and aluminum, Journal of Vacuum Science & Technology A: Vacuum, Surfaces, and Films. 5 (1987) 2173–2179, https://doi.org/10.1116/1.574948.

[13] W.D. Sylwestrowicz, Oxidation of titanium thin films, J. Electrochem. Soc. 122 (1975) 1504–1508, https://doi.org/10.1149/1.2134053.

[14] D. McIntyre, J.E. Greene, G. Håkansson, J.-E. Sundgren, W.-D. Münz, Oxidation of metastable single-phase polycrystalline Ti $_{0.5}$ Al $_{0.5}$ N films: Kinetics and mechanisms, J. Appl. Phys. 67 (1990) 1542–1553, https://doi.org/10.1063/1.345664.

[15] G. Greczynski, L. Hultman, M. Odén, X-ray photoelectron spectroscopy studies of Ti1-Al N ($0 \leq x \leq 0.83$) high-temperature oxidation: The crucial role of Al concentration, Surf. Coat. Technol. 374 (2019) 923–934, https://doi.org/10.1016/j.surfcoat.2019.06.081.

[16] L. Chavee, E. Serag, M. da Silva Pires, S. Lucas, E. Haye, A mechanistic approach of oxidation resistance, structural and mechanical behaviour of TiAlN coatings, Appl. Surf. Sci. 586 (2022) 152851, https://doi.org/10.1016/j.apsusc.2022.152851.

[17] C. Gnoth, C. Kunze, M. Hans, M. to Baben, J. Emmerlich, J.M. Schneider, G. Grundmeier, Surface chemistry of TiAlN and TiAlNO coatings deposited by means of high power pulsed magnetron sputtering, J. Phys. D: Appl. Phys. 46 (2013) 084003, https://doi.org/10.1088/0022-3727/46/8/084003.

[18] G. Greczynski, S. Mráz, L. Hultman, J.M. Schneider, Venting temperature determines surface chemistry of magnetron sputtered TiN films, Appl. Phys. Lett. 108 (2016) 041603, https://doi.org/10.1063/1.4940974.

[19] C. Kunze, D. Music, M. to Baben, J.M. Schneider, G. Grundmeier, Temporal evolution of oxygen chemisorption on TiAlN, Appl. Surf. Sci. 290 (2014) 504–508, https://doi.org/10.1016/j.apsusc.2013.11.091.

[20] D. Music, J.M. Schneider, *Ab initio* study of Ti $_{0.5}$ Al $_{0.5}$ N(001)—residual and environmental gas interactions, New J. Phys. 15 (2013) 073004, https://doi.org/10.1088/1367-2630/15/7/073004.

[21] P.H. Mayrhofer, A. Hörling, L. Karlsson, J. Sjölén, T. Larsson, C. Mitterer, L. Hultman, Self-organized nanostructures in the Ti–Al–N system, Appl. Phys. Lett. 83 (2003) 2049–2051, https://doi.org/10.1063/1.1608464.

[22] H. Brongersma, M. Draxler, M. Deridder, P. Bauer, Surface composition analysis by low-energy ion scattering, Surf. Sci. Rep. 62 (2007) 63–109, https://doi.org/10.1016/j.surfrep.2006.12.002.

[23] T. Fauster, Surface geometry determination by large-angle ion scattering, Vacuum 38 (1988) 129–142, https://doi.org/10.1016/0042-207X(88)90611-2.

[24] D. Primetzhofer, S.N. Markin, R. Kolarova, M. Draxler, R. Beikler, E. Taglauer, P. Bauer, On the surface sensitivity of angular scans in LEIS, Nucl. Instrum. Methods Phys. Res., Sect. B 258 (2007) 36–39, https://doi.org/10.1016/j.nimb.2006.12.176.

[25] D. Primetzhofer, S.N. Markin, P. Zeppenfeld, P. Bauer, S. Prusa, M. Kolibal, T. Sikola, Quantitative analysis of ultra thin layer growth by time-of-flight low energy ion scattering, Appl. Phys. Lett. 92 (2008) 011929, https://doi.org/10.1063/1.2822816.

[26] D. Primetzhofer, M. Spitz, S.N. Markin, E. Taglauer, P. Bauer, Influence of surface structure and composition on neutralization of H 4 e + ions scattered from noble metals and alloy surfaces, Phys. Rev. B. 80 (2009) 125425, https://doi.org/10.1103/PhysRevB.80.125425.

[27] P.M. Wolf, E. Pitthan, Z. Zhang, C. Lavoie, T.T. Tran, D. Primetzhofer, Direct transition from ultrathin orthorhombic dinickel silicides to epitaxial nickel disilicide revealed by in situ synthesis and analysis, Small 18 (2022) 2106093, https://doi.org/10.1002/smll.202106093.

[28] P. Ström, D. Primetzhofer, Ion beam tools for nondestructive in-situ and in-operando composition analysis and modification of materials at the tandem laboratory in uppsala, J. Inst. 17 (2022) P04011, https://doi.org/10.1088/1748-0221/17/04/P04011.

[29] V. Kouznetsov, K. Macák, J.M. Schneider, U. Helmersson, I. Petrov, A novel pulsed magnetron sputter technique utilizing very high target power densities, Surf. Coat. Technol. 122 (1999) 290–293, https://doi.org/10.1016/S0257-8972(99)00292-3.

[30] G. Greczynski, S. Mráz, M. Hans, D. Primetzhofer, J. Lu, L. Hultman, J. M. Schneider, Unprecedented Al supersaturation in single-phase rock salt structure VAlN films by Al $^+$ subplantation, Journal of Applied Physics. 121 (2017) 171907, https://doi.org/10.1063/1.4977813.

[31] M. Draxler, S.N. Markin, S.N. Ermolov, K. Schmid, C. Hesch, A. Poschacher, R. Gruber, M. Bergsmann, P. Bauer, ACOLISSA: A powerful set-up for ion beam analysis of surfaces and multilayer structures, Vacuum 73 (2004) 39–45, https://doi.org/10.1016/j.vacuum.2003.12.041.

[32] J.P. Biersack, E. Steinbauer, P. Bauer, A particularly fast TRIM version for ion backscattering and high energy ion implantation, Nucl. Instrum. Methods Phys. Res., Sect. B 61 (1991) 77–82, https://doi.org/10.1016/0168-583X(91)95564-T.

[33] J.P. Biersack, L.G. Haggmark, A Monte Carlo computer program for the transport of energetic ions in amorphous targets, Nucl. Inst. Methods 174 (1980) 257–269, https://doi.org/10.1016/0029-554X(80)90440-1.

[34] J.F. Ziegler, M.D. Ziegler, J.P. Biersack, SRIM - The stopping and range of ions in matter (2010), Nucl. Instrum. Methods Phys. Res., Sect. B 268 (2010) 1818–1823, https://doi.org/10.1016/j.nimb.2010.02.091.

[35] J.F. Ziegler, J.P. Biersack, U. Littmark, The Stopping and Range of Ions in Solids, Pergamon Press Inc, New York, 1985.

[36] D. Primetzhofer, S. Rund, D. Roth, D. Goebl, P. Bauer, Electronic excitations of slow ions in a free electron gas metal: Evidence for charge exchange effects, Phys. Rev. Lett. 107 (2011) 163201, https://doi.org/10.1103/PhysRevLett.107.163201.

[37] L.E. Davis, N.C. MacDonald, P.W. Palmberg, G.E. Riach, R.E. Weber, Handbook of Auger electron spectroscopy: A reference book of standard data for identification and interpretation of Auger electron spectroscopy data, 2nd Edition, Physical Electronics Industries, Eden Prairie. Minnesota 55343, 1976.

[38] M. Draxler, R. Beikler, E. Taglauer, K. Schmid, R. Gruber, S.N. Ermolov, P. Bauer, Explanation of the surface peak in charge integrated LEIS spectra, Nucl. Instrum. Methods Phys. Res. Sect. B-Beam Interact. Mater. Atoms 203 (2003) 218–224, https://doi.org/10.1016/S0168-583X(02)02220-6.

[39] K. Oura, M. Katayama, A.V. Zotov, V.G. Lifshits, A.A. Saranin, Surface Science, Springer, Berlin Heidelberg, Berlin, Heidelberg (2003), https://doi.org/10.1007/978-3-662-05179-5.

[40] E. Pitthan, M.V. Moro, S.A. Corrêa, D. Primetzhofer, Assessing boron quantification and depth profiling of different boride materials using ion beams, Surf. Coat. Technol. 417 (2021) 127188, https://doi.org/10.1016/j.surfcoat.2021.127188.

[41] C.N.R. Rao, D.D. Sarma, M.S. Hegde, A novel approach to the study of surface oxidation states and oxidation of transition metals by Auger electron spectroscopy, Proc. R. Soc. Lond. A. 370 (1980) 269–280, https://doi.org/10.1098/rspa.1980.0033.

[42] I. Vaquila, L.I. Vergara, M.C.G. Passeggi, R.A. Vidal, J. Ferrón, Chemical reactions at surfaces: Titanium oxidation, Surf. Coat. Technol. 122 (1999) 67–71, https://doi.org/10.1016/S0257-8972(99)00420-X.

[43] M. Hans, P. Keuter, A. Saksena, J.A. Sälker, M. Momma, H. Springer, J. Nowak, D. Zander, D. Primetzhofer, J.M. Schneider, Opportunities of combinatorial thin film materials design for the sustainable development of magnesium-based alloys, Sci Rep. 11 (2021) 17454, https://doi.org/10.1038/s41598-021-97036-6.

[44] X. Chen, B. Stelzer, M. Hans, R. Iskandar, J. Mayer, J.M. Schneider, Enhancing the high temperature oxidation behavior of Cr $_2$ AlC coatings by reducing grain boundary nanoporosity, Materials Research Letters. 9 (2021) 127–133, https://doi.org/10.1080/21663831.2020.1854358.

[45] M. Hans, Z. Czigány, D. Neuß, J.A. Sälker, H. Rueß, J. Krause, G.K. Nayak, D. Holec, J.M. Schneider, Probing the onset of wurtzite phase formation in (V, Al)N thin films by transmission electron microscopy and atom probe tomography, Surf. Coat. Technol. 442 (2022) 128235, https://doi.org/10.1016/j.surfcoat.2022.128235.

[46] F. Adibi, I. Petrov, L. Hultman, U. Wahlström, T. Shimizu, D. McIntyre, J.E. Greene, J.-E. Sundgren, Defect structure and phase transitions in epitaxial metastable cubic Ti $_{0.5}$ Al $_{0.5}$ N alloys grown on MgO(001) by ultra-high-vacuum magnetron sputter deposition, J. Appl. Phys. 69 (1991) 6437–6450, https://doi.org/10.1063/1.348849.

[47] Y. Yamamura, N. Matsunami, N. Itoh, Theoretical studies on an empirical formula for sputtering yield at normal incidence, Radiat. Eff. 71 (1983) 65–86, https://doi.org/10.1080/00337578308218604.

[48] N. Matsunami, Y. Yamamura, Y. Itikawa, N. Itoh, Y. Kazumata, S. Miyagawa, K. Morita, R. Shimizu, H. Tawara, Energy dependence of the ion-induced sputtering yields of monatomic solids, At. Data Nucl. Data Tables 31 (1984) 1–80, https://doi.org/10.1016/0092-640X(84)90016-0.

[49] D.M. Holzapfel, D. Music, M. Hans, S. Wolff-Goodrich, D. Holec, D. Bogdanovski, M. Arndt, A.O. Eriksson, K. Yalamanchili, D. Primetzhofer, C.H. Liebscher, J. M. Schneider, Enhanced thermal stability of (Ti, Al)N coatings by oxygen incorporation, Acta Mater. 218 (2021) 117204, https://doi.org/10.1016/j.actamat.2021.117204.